OPTICS OF ERYTHROCYTES

Peter Tarasov,[1] Maxim Yurkin,[1,2] Pavel Avrorov,[1,3] Konstantin Semyanov,[1] Alfons Hoekstra,[2] and Valeri Maltsev[1,3]
[1]*Institute of Chemical Kinetics and Combustion, Institutskaya 3, Novosibirsk,630090, Russia;*
[2]*Faculty of Science, Section Computational Science, of the University of Amsterdam, Kruislaan 403, 1098 SJ, Amsterdam, The Netherlands;*
[3]*Novosibirsk State University Pirogova 3, Novosibirsk,630090, Russia;*

Abstract: We present optical methods to study erythrocytes and consider selected models to compute their light scattering.

Key words: erythrocyte, cassini, DDA

1. INTRODUCTION

Light-scattering properties of blood depend on the optical properties of red blood cells (RBC) because these cells form the disperse phase of blood. Moreover, the importance of RBC volume and hemoglobin concentration in clinical hematological analysis also emphasizes their importance. RBCs also play an important role in verification of solutions of the direct light-scattering problem for non-spherical particles because of their simple internal structure and stable biconcave discoid shape. Nevertheless the large size to wavelength ratio for an individual RBC (approximately 40) encourages the use of approximations in light-scattering theory and/or simplifying the shape in order to simulate light scattering from individual RBCs. For instance, RBCs have been assumed to be volume equivalent spherical,[1,2] spheroidal,[3] or ellipsoidal,[4,5] dielectric particles. Such assumptions can only be valid under special experimental conditions, such as isovolumetric sphering, osmotic swelling or deformation in shear flow. Approximate theories, such as Fraunhofer and anomalous diffraction theories,[4] Wentzel-Kramers-Brillouin[6] or physical optics[5] approximations

A. Hoekstra et al. (eds.), Optics of Biological Particles, 243–259.

can only be satisfactorily used for studies of the formation of structure peculiarities in the light-scattering patterns of individual RBCs. These approximations could not be applied in the solution of the inverse light-scattering problem to determine the RBC characterisitics from light-scattering data.

Tsinopoulos and Polyzos[7] were the first to rigorously simulate light scattering by realistic non-deformed RBCs. They used a boundary element method appropriately combined with fast Fourier transform (FFT) algorithms. This method also was applied to aggregated red blood cells.[8] Another method that employs rotational symmetry of RBCs is the Discrete Sources Method (DSM), which was applied to RBC light scattering by Eremina *et al.*,[9] who compared a realistic shape with spheroids and disc-spheres. Comparing the light-scattering profiles of biconcave disc-shaped RBC and approximating shapes, this study provided a determination of boundaries of usage of the approximating shapes in simulation of light scattering from mature RBCs. Most important conclusions are as follows:

1. The approximation of a RBC with a volume-equivalent sphere is not accurate.
2. The approximation of a RBC with a size–volume-equivalent oblate spheroid can be considered satisfactory for only the case of face-on incidence and quite successful only when one is interested in collecting data close to the forward direction, $\theta \leq \sim 4°$.
3. The scattering properties of a RBC are not essentially affected by the presence of the surrounded membrane.
4. The disk-sphere model of a RBC gives better agreement with the biconcave disk model comparedd with the spheroid model.

While methods employing the axisymmetric properties of RBCs are the fastest, more general and widespread methods suitable for arbitrary-shaped scatterers, such as the Discrete Dipole Approximation (DDA) and the Finite Difference Time Domain method (FDTD), have recently been applied to RBC scattering. Karlsson *et al.*[10] studied light scattering by RBCs with FDTD (λ from 600 to 1000 nm in vacuum), DDA (used only for validation of FDTD) and different approximate methods (Rytov approximation, superposition method). These approximate methods agree well with FDTD for small scattering angles. A similar analysis was done for two touching RBCs.[11] Another FDTD study of RBC light scattering (λ = 633nm in vacuum) was performed by Lu *et al.*[12] (see also their chapter in this volume). They used a simple geometrical parameterization of the RBC shape[13] and studied effects of varying RBC shape, orientation, and the wavelength of the incident beam. Moreover, they also studied light scattering by RBCs deformed in blood flow,[14] using a more advance parallel FDTD code.

Numerical results for the angular distributions of the Mueller scattering matrix elements of an RBC and their dependence on shape, orientation, and wavelength are presented.

Yurkin *et al.*[15] applied DDA to simulate light scattering by a RBC and compared this with experimental light-scattering patterns measured by a Scanning Flow Cytometer (SFC). A good agreement could be demonstrated, thus validating the biconcave disk model[16] for a mature RBC. Moreover, this allowed the authors to solve the inverse light-scattering problem, resulting in the determination of a RBC's diameter, volume and orientation in the flow from the measured SFC signal. Finally, scattering from the biconcave disk shape was compared with that of the spheroid and disc-sphere models. The conclusion of this[15] and other[9,11] papers was that simplified geometrical shapes models of RBCs are generally unsatisfactory.

A detailed comparison of simulations by different authors is hindered by the fact that slightly different shape models are used for a native non-deformed RBC. Most papers[7,8,10,11,15] describe a model based on the microscopic measurements by Fung *et al.*[16] where an empirical polynomial fit for hypothetical intersample–averaged human cells is reported. Other shape models are due to Skalak *et al.*[17] (used by Shvalov *et al.*[6] and Eremina *et al.*[9]), a parametric model by Borovoi *et al.*[13] (used by Lu *et al.*[12]), and a surface of rotation of a Cassini curve.[5] In many particular cases all these approximate shape models may lead to the same satisfactory results. However, the validity of such shape models for the calculation of scattering by RBCs should be further studied for different sizes, and within the context of the specific application in which such scattering results are to be used.

Until recently, the characterization of an erythrocyte population (in terms of volume distributions and hemoglobin concentrations) was achieved by isovolumetric sphering of the cells, followed by a 2-angular scattering measurement. This allows an efficient measurement of the mutual distribution of RBC volume and hemoglobin concentration.[18,19] In the consequent sections new approaches to characterize erythrocytes from light scattering, with emphasis on application of scanning flow cytometry, are considered.[20]

2. STATIC CHARACTERIZATION OF INDIVIDUAL ERYTHROCYTES

Classical flow cytometry of red cells uses low-angular and 90-degree scattering in combination with fluorescence.[21] The low-angular scattering is

thought to correlate with cell size. The main purpose of fluorescence is to discriminate between red cells and other cell types. A qualitative analysis of the resulting light scattering histograms, in combination with fluorescence results in important information about the mechanism of erythrocyte aging *in vivo*.[22,23,24]

2.1 Scanning Flow Cytometer

A scanning flow cytometer[20,25] (SFC) sufficiently extends the capabilities of flow cytometry in the morphological characterization of RBCs by measuring angularly resolved light-scattering profiles (LSP) of individual cells. The current set-up of the SFC provides measurement of the following combination of Mueller matrix elements:

$$I(\theta) = \int_0^{2\pi} [S_{11}(\theta,\varphi) + S_{14}(\theta,\varphi)] d\varphi \quad (1)$$

where $I(\theta)$ is the output signal of the SFC, θ and φ are the polar and azimuthal angles, with respect to incident radiation. A typical range of θ is from 5^0 to 80^0. The second term in the integral is zero for particles having a symmetry plane that contains the propagation vector of the incident beam.[15] For arbitrary shaped particles this term is negligible.

Absorption of hemoglobin is very small for the wavelength of incident radiation used in this study (0.6328 μm). Variations in the real part of the refractive index between erythrocytes can be attributed solely to variations in hemoglobin concentration.[2] Absorption of hemoglobin is caused by an uncontrolled level of oxygenation variations. At the given wavelength, absorption can be neglected ($\sim 10^{-5}$).

2.2 RBC Sampling

Whole blood was taken from a healthy volunteer by venopuncture with EDTA as anticoagulant and resuspended in buffered saline (0,01M HEPES buffer (Sigma), pH 7.4 with 0.15M NaCl). For the acid hemolysis erythrocytes were resuspended in 0.15M NaCl without buffer. Then the cells were stored at room temperature (23^0C) and used within three hours. Longer storage significantly affects kinetics of hemolysis and the volume of the cells. Experiments were also carried out at room temperature. All blood samples were taken from the same individual to allow for comparison.

Murine cells were obtained from anaesthetized mice of a C57Bl6 line by cardiac puncture and were processed in the same manner. Murine cells were used to demonstrate the applicability of the analysis over a wide range of sizes.

2.3 Isovolumetric Sphering

Isovolumetric sphering in the presence of SDS (sodium dodecyl sulfate) was applied to attain a spherical shape of the cells.[18] The sphering close to ideal is achieved by balancing the weight ratio of SDS/protein at approximately 1/50 or less. The use of endogenous serum protein is possible: the dilution of the whole blood 1/50 in phosphate buffer saline with 0.003% SDS for a minute and consequent dilution 1/25 by isotonic saline of 0.1% glutaraldehyde and 0.001% SDS. The modification of the method has been chosen where 0.1% human serum albumin is present in the surrounding isotonic medium as a protecting agent and SDS concentration is 0.004%.

2.4 Lysing Procedures

A volume containing 4μl of solution with erythrocytes was placed into a test-tube with 1ml of lysing solution to achieve a final concentration in the range of 5×10^5 – 2×10^7 cells/ml. To ensure homogeneity of cell concentrations the samples have been swirled for 2-3 seconds with a vortex mixer or stirred up by pipetting. The overall delay between introduction of a sample to lysing solution and start of measurements constituted about 15-20 seconds.

Isotonic ammonium chloride is a widespread erythrocyte lysing solution.[26] The process of lysis is mediated by Jacobs Stewart's cycle[27] and based on transport properties of band 3 protein, which is present on mammalian RBCs. At present there is no complete mathematical model for this type of lysis.

A typical composition of commercial lysing solution is as follows: NH_4Cl (0.15M), $NaHCO_3$ (~10 mM), disodium EDTA (~1 mM), pH=7.4. Ammonium chloride acts as equilibrating agent increasing intracellular osmolyte content.[28] Dissolved CO_2 - HCO_3^- pair performs a "catalysing" role with saturating concentrations of about 5 mM.[29] At these concentrations a typical time of hemolysis is less than a minute, rather fast in comparison to the delay required to prepare a sample. Usually in "hand-made" lysing solutions the addition of HCO_3^- ions is omitted, taking advantage of only atmospheric CO_2 dissolved in water. At these conditions the whole process lasts about 5 minutes.

We have chosen the following modification of lysing solution: addition of controlled intermediate concentrations of HCO_3^- ions (1 mM) in the form of sodium salt to degassed water (boiled in a microwave for 10 minutes), isotonic concentration of NH_4Cl with 1.5mM buffer HEPES (Sigma). The resulting solution has buffer properties with pH ~ 7.2. Solutions prepared in this manner have been used for an hour.

2.5 Osmotic Fragility Test

The osmotic fragility was performed in a classical manner placing an aliquot of a stock solution of blood into a series of saline solutions of decreasing ionic strength with consequent calculation of a percentage of hemolysis. The lysis percentage was determined by measurement of the optical density of hemoglobin in supernatants. Measurements were performed using a microculture plate reader (Behring ELISA Processor II, Behringwerke, AG Diagnostica, Germany) at wavelengths of 570, 492, 450 nm to verify absence of variation between samples caused by oxygenation degree. Triplicate samples were tested at each concentration of saline. Hemolysis was expressed as a percentage of hemoglobin released in distilled water. Optical corrections for differences in concentration of saline were taken into account.

2.6 Method of Spectral Decomposition

In order to provide an effective comparison of experimental and theoretical light-scattering data, the LSPs are modified[30, 31] by multiplication with the weighting function $f(\theta)$ defined as

$$F(\theta) = f(\theta) \cdot I(\theta) = \sin^2\left(\pi \frac{\theta - \theta_l}{\theta_h - \theta_l}\right) \cdot I(\theta) \tag{2}$$

where θ_l and θ_k are the minimal and maximal significant scattering angles of the measured LSP. Typical values are θ_l = 10° and θ_h = 70°. The multiplication corresponds to a standard Hanning window procedure that strongly reduces the effects of discontinuities at the beginning and end of the sampling period of the SFC. Moreover, this function resembles the SFC instrument function[25] and improves visual inspection of LSPs as the logarithmic scale can be substituted with a linear one. Peaks emerge in the frequency domain of the *modified LSP*, corresponding to light-scattering resonance on characteristic dimensions of the particle (*Figure 1*).

The following empirical equation was derived to connect the location of the peak in the spectrum of modified light scattering LSP and the size parameter of a homogeneous spherical particle:[31]

$$\alpha = C_1 \cdot P_f \tag{3}$$

where the coefficient C_1 is ~ 189.12 for the given wavelength, $\alpha = m_0 \pi d/\lambda$, d is the particle diameter, m_0 is the refractive index of the medium, λ is the wavelength of incident light in vacuum, P_f is the position of the spectral peak. This equation gives a precision of 3% sizing a homogeneous spherical particle with refractive indices in the region from 1.37 to 1.70. This region of refractive indices covers the refractive indices of biological cells.

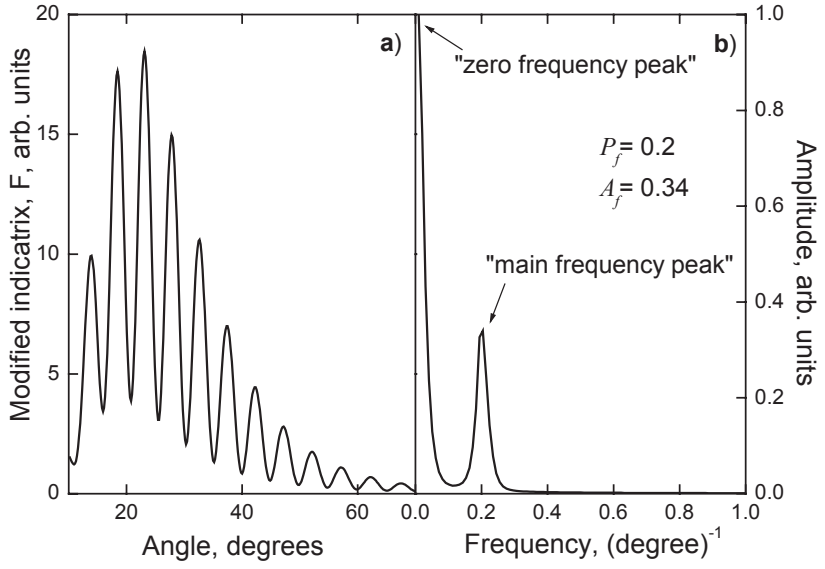

Figure 1. Modified LSP $F(\theta)$ (a) of a spherical particle (diameter 5.7 μm, refractive index 1.39) and its normalized Fourier spectrum (b), where P_f is the location and A_f is the amplitude of the main frequency peak.

2.6.1 Characterization of spherical RBC

The parametric solution of the inverse light-scattering problem for sphered erythrocytes is based on two parameters[32]: P_f and the integral of the modified LSP, denoted by J.

$$J = \int_{\theta_l}^{\theta_h} f(\theta) \cdot I(\theta) d\theta$$

$$V^{1/3} \propto r_{sphere} \propto P_f \tag{4}$$

$$HBC = \frac{n_R - n_0}{\beta} \propto J^{const} / P_f \; ; const \approx 0.43$$

Here V and HBC are the volume and the hemoglobin concentration of a spherical particle, respectively, r_{sphere} is the radius of the particle, β is the coefficient expressed in dL/g, n_R is the real part of refractive index of a cell and n_0 is the refractive index of the surrounding medium, β has a typical value of 0.0019 dL/g.[2]

The inversion algorithm is applicable to cells with spherical shape and volumes ranging from 30 μm^3 to 250 μm^3 and hemoglobin concentrations from 5 to 50 g/dL.[32] With this method we analyzed murine and human RBCs to determine the distributions of cell volume and hemoglobin concentration. Two-dimensional contour plot shown in *Figure 2* demonstrates the results of the analysis.

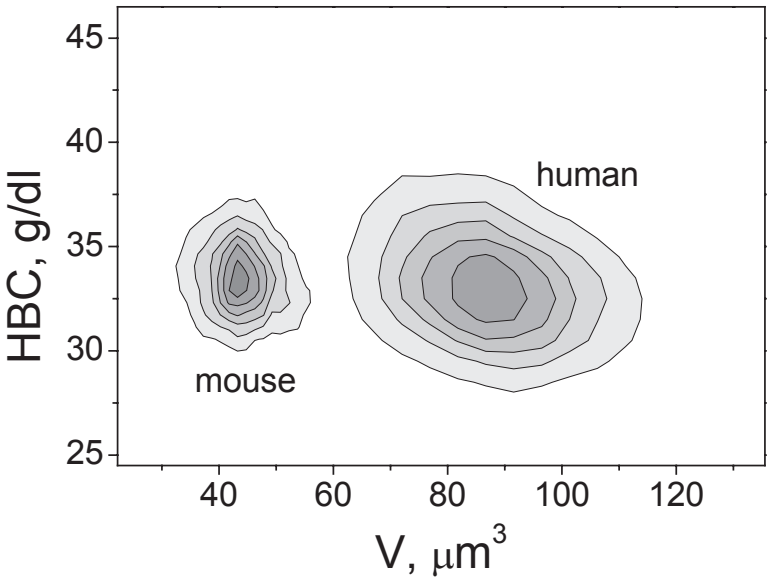

Figure 2. Two hematological indices of RBCs of human and mouse measured with SFC after isovolumetric sphering.

2.6.2 Recognition of spherical particles

Common practice to determine RBC size and hemoglobin concentration, as implemented in commercial analyzers, utilizes measurement over two spatial angles in the forward directions.[2] This method allows characterization of spherized RBCs only. On the other hand this method does not distinguish between spherical and non-spherical cells, resulting in an uncertainty in determination of RBC characteristics. The LSPs of individual RBCs, as measured with the SFC, provide the possibility to recognize spherical cells before their characterization. We calculate the LSPs of oblate spheroids using the T-matrix method[33] for spheroid

characteristics congruent with typical RBCs. We find that the amplitude of the peak A_f of the normalized Fourier spectrum (i.e. the spectrum divided by the amplitude of the zero frequency peak) correlates with the aspect ratio of the spheroid. To model the conversion of an erythrocyte to a sphere, we assume an increase in volume of the spheroid while keeping the surface area constant (i.e. sphering in late stages of hemolysis). For our computations we use the available T-matrix code.[34] Sphering of three spheroids with initial characteristics equal to a typical average and two extreme values of V_0, and HBC_0 have been simulated. The results shown in *Figure 3* allow us to conclude that erythrocyte shape could be classified as a sphere if $A_f > 0.25$. This algorithm recognizes spheroids with aspect ratio $\varepsilon \geq 0.93$.

This algorithm allows us to estimate the error caused by non-sphericity $\varepsilon \geq 0.93$ of the RBC in the determination of RBC characteristics with the spectral decomposition approach. We define the error in computation of the volume of a spheroid as

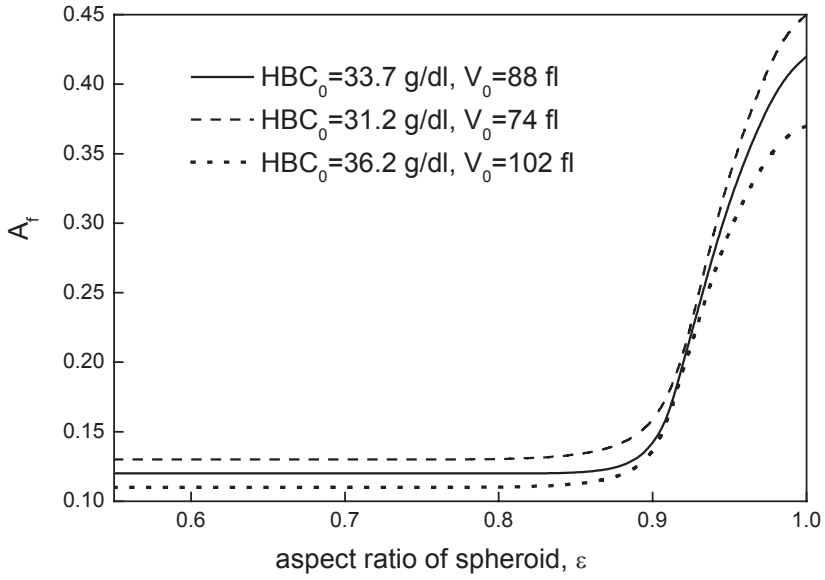

Figure 3. Amplitude of the main frequency peak A_f as a function of aspect ratio ε of a spheroid. Graphs for mean and bounding values of RBC characteristics (V_0, HBC_0) are shown.

$$Error_V = \left| V_{calc} - V_{theor} \right| / V_{theor} \quad (5)$$

where V_{theor} is the volume of spheroid used in the simulations, and V_{calc} the volume obtained from the solution of the inverse problem, using model LSPs. The error was estimated for 200 theoretical LSPs of spheroids with ε ranging from 0.6 to 1, hemoglobin concentrations were 18.2, 28.9, 39.3 g/dL. The range of volumes was varied from 70 to 180 femtoliters. The resulting $Error_V$ as function of the aspect ratio is shown in *Figure 4*(a).

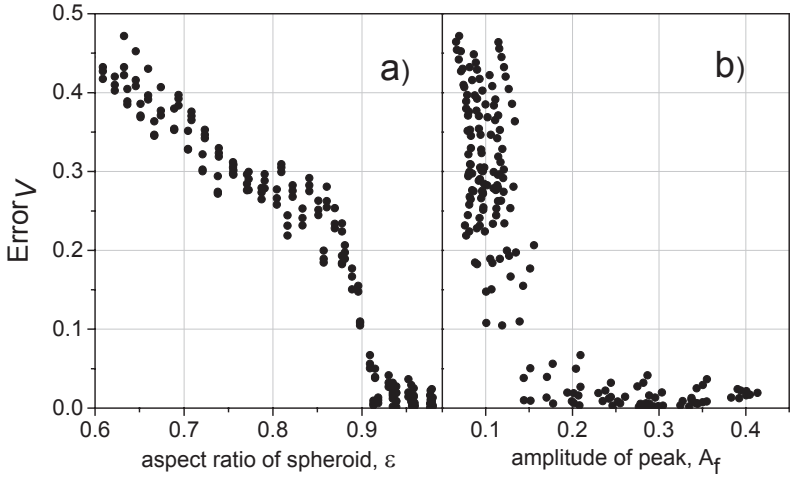

Figure 4. Error of RBC volume as a function of a) spheroid aspect ration and b) amplitude of the main frequency peak.

The results shown in *Figure 4* allow us to fix the threshold in the amplitude of the peak A_f such that the RBC volume is determined with an error smaller than 5%. The amplitude of the peak must exceed 0.25.

Our approach allows us to estimate the fraction of non-spherical RBCs remaining during spherization. The amplitude of the spectral peak on spheroid aspect ratio calculated for typical RBC characteristics with the T-matrix method is shown in *Figure 5*a). The distribution of the amplitudes of the spectral peak for isovolumetrically sphered RBCs measured with the SFC is shown in *Figure 5*b). The data shown in *Figure 5* demonstrate that at least a part of the erythrocytes is not spherical. Nevertheless, the value of A_f is larger than 0.2 for all cells, and the population can be characterized by our algorithm with precision in volume and concentration of hemoglobin of ~5%. Parameters obtained from this isovolumetric sphering experiments are

$\overline{V}_0$=87.1, w_{V_0}=10.2, $\overline{HBC_0}$=33.4, w_{HBC_0}=2.11, where w_{V_0} and w_{HBC_0} are the width of the distribution of RBC volume and hemoglobin concentration, respectively.

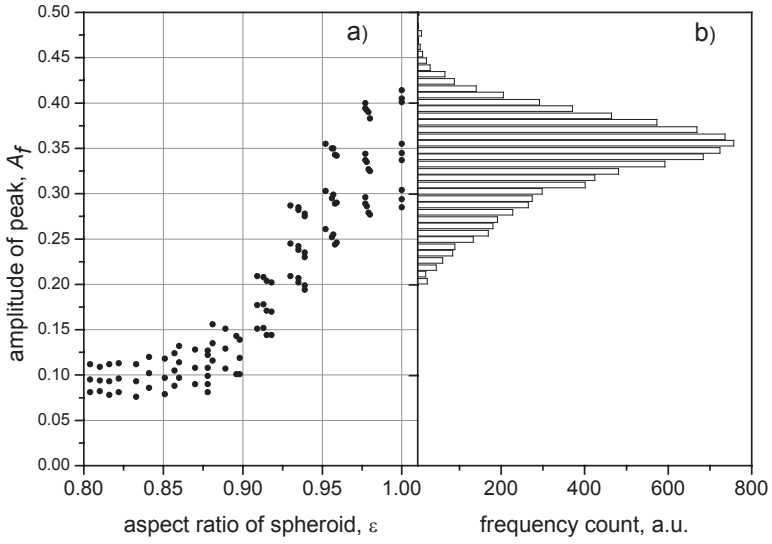

Figure 5. The amplitude of spectral peak as a function of spheroid aspect ratio calculated for typical RBC characteristics with T-matrix method a) and distribution of amplitude of spectral peak for isovolumetric sphered RBC measured with SFC.

2.6.3 Diameters of mature erythrocytes

The LSP structure of mature RBCs is sensitive to the RBC characteristics that may allow us to solve the inverse light-scattering problem to determine the RBC diameters from measured LSPs. We applied the spectral decomposition approach to relate the RBC diameter with a proper LSP parameter. This relation was discovered from simulations of light-scattering from biconcave disks using the Discrete Dipole Approximation (DDA).[15] The LSPs and spectra were calculated for a cell volume of 100 fl and for different cell diameters ranging from 6.75 μm to 8.28 μm. The results of three representative simulations are shown in *Figure 6*. The symmetry axes of the disks were orthogonal to the direction of the incident laser beam. There are a few peaks in the spectra. We found that the location of the "last" essential peak (in the scale of degrees^{-1}) corresponds to the diameter of the red blood cell.

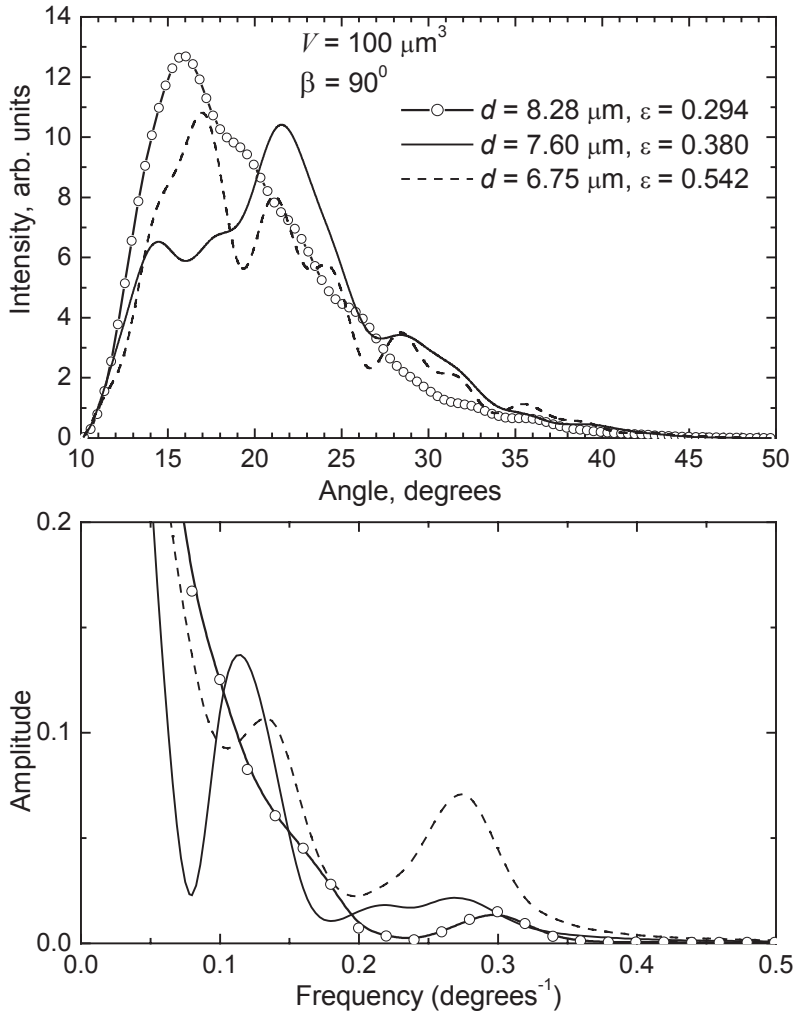

Figure 6. Modified theoretical light scattering LSPs (top) and their spectra (bottom) for biconcave disks of the three different shapes. V is the volume and d the diameter of the erythrocyte, ε is the ratio of the erythrocyte's thickness to diameter d. Cells are elongated along the direction of the incident laser beam.

In order to define in an unambiguous way this last essential peak we have to exclude the effect of background noise. The noise is due to laser noise of 0.5 % of the total power under current experimental conditions. A

considerable contribution to the noise for weak signals is caused by quantization noise of the analog-to-digital converter. This part was easily measured in the absence of a light-scattering signal and was 0.0006 in arbitrary units. The total noise level can be calculated by $L=0.005\times M + 0.0006$, where M is the mean value of the measured signal. The essential peaks are defined as those peaks exceeding the noise level.

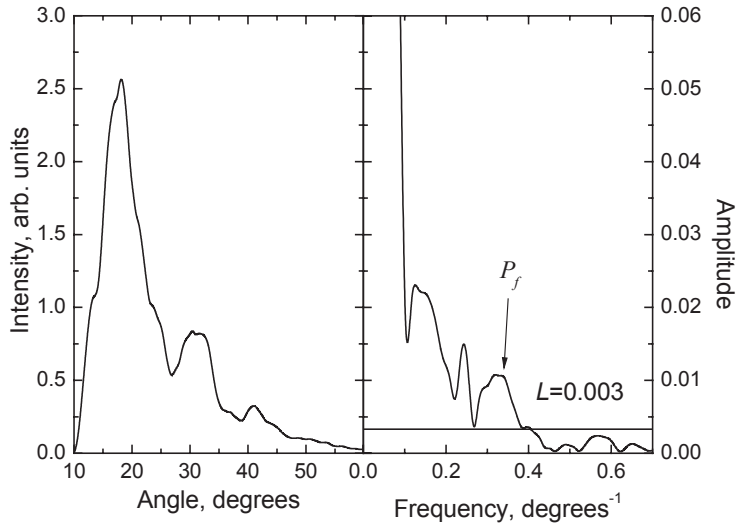

Figure 7. A typical experimental LSP (left) of a mature RBC with its spectrum (right). Calculated noise level L and the position of the last essential peak P_f are shown.

A typical LSP of an erythrocyte and its associated spectrum are shown in Figure 7. The location of the last essential peak has been used in equation (3) to calculate diameter of erythrocytes, d. Four thousand LSPs of mature RBCs were proceesed with this method and the resulting distribution of RBC diameters is shown in Figure 8. The mean diameter and width of the distribution are slightly different from the distribution parameters introduced by Fung *et al.*[16] but the maximal and minimal diameters of both distributions are in good agreement. These results demonstrate the performance of the SFC and the spectral decomposition method to be a basis of a new hematological index – RBC diameter that can be determined in automatic regime.

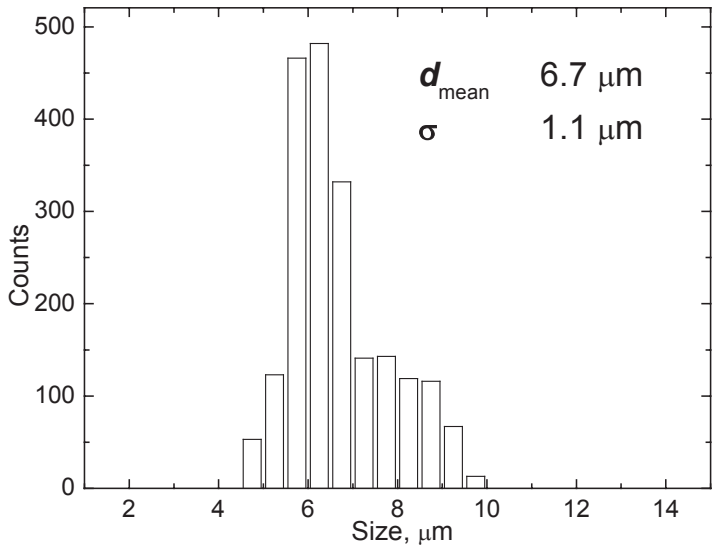

Figure 8. The diameter distribution of mature RBCs measured with SFC.

3. CONCLUSION

In this work we have illustrated how the SFC, in combination with a proposed inversion algorithm and common *in vitro* procedures can help to expand characterization of individual RBCs. For isovolumetric sphering, which is widespread in hematology analyzers, SFC provides the ability to monitor aspect ratios of swollen cells.

REFERENCES

1. J. M. Steinke and A. P. Shepherd, Comparison of mie theory and the light-scattering of red blood-cells, *Appl. Opt.* **27**, 4027-4033 (1988).
2. D. H. Tycko, M. H. Metz, E. A. Epstein, and A. Grinbaum, Flow-cytometric light scattering measurement of red blood cell volume and hemoglobin concentration, *Appl. Optics.* **24**, 1355-1365 (1985).

3. A. M. K. Nilsson, P. Alsholm, A. Karlsson, and S. Andersson-Engels, T-matrix computations of light scattering by red blood cells, *Appl. Optics*. **37**, 2735-2748 (1998).
4. G. J. Streekstra, A. G. Hoekstra, E. J. Nijhof, and R. M. Heethaar, Light scattering by red blood cells in ektacytometry: Fraunhofer versus anomalous diffraction, *Appl. Opt.* **32**, 2266-2272 (1993).
5. P. Mazeron and S. Muller, Light scattering by ellipsoids in a physical optics approximation, *Appl. Opt.* **35**, (1996).
6. A. N. Shvalov, J. T. Soini, A. V. Chernyshev, P. A. Tarasov, E. Soini, and V. P. Maltsev, Light-scattering properties of individual erythrocytes, *Appl. Opt.* **38**, 230-235 (1999).
7. S. V. Tsinopoulos and D. Polyzos, Scattering of He-Ne laser light by an average-sized red blood cell, *Appl. Opt.* **38**, 5499-5510 (1999).
8. S. V. Tsinopoulos, E. J. Sellountos, and D. Polyzos, Light scattering by aggregated red blood cells, *Appl. Opt.* **41**, 1408-1417 (2002).
9. E. Eremina, Y. Eremin, and T. Wriedt, Analysis of light scattering by erythrocyte based on discrete sources method, *Opt. Comm.* **244**, 15-23 (2005).
10. A. Karlsson, J. P. He, J. Swartling, and S. Andersson-Engels, Numerical simulations of light scattering by red blood cells, *IEEE Trans. Biomed. Engin.* **52**, 13-18 (2005).
11. J. He, A. Karlsson, J. Swartling, and S. Andersson-Engels, Light scattering by multiple red blood cells, *J. Opt. Soc. Am. A* **21**, 1953-1961 (2004).
12. J. Q. Lu, P. Yang, and X. Hu, Simulations of light scattering from a biconcave red blood cell using the finite-difference time-domain method, *J. Biomed. Opt.* **10**, 024022 (2005).
13. A. G. Borovoi, E. I. Naats, and U. G. Oppel, Scattering of light by a red blood cell, *J. Biomed. Opt.* **3**, 364-372 (1998).
14. R. S. Brock, X. Hu, P. Yang, and J. Q. Lu, Evaluation of a parallel FDTD code and application to modeling of light scattering by deformed red blood cells, *Opt. Expr.* **13**, 5279-5292 (2005).
15. M. A. Yurkin, K. A. Semyanov, P. A. Tarasov, A. V. Chernyshev, A. G. Hoekstra, and V. P. Maltsev, Experimental and theoretical study of light scattering by individual mature red blood cells with scanning flow cytometry and discrete dipole approximation, *Appl. Opt*. **44**, 5249-5256 (2005).
16. Y. C. Fung, W. C. Tsang, and P. Patitucci, High-resolution data on the geometry of red blood cells, *Biorheology* **18**, 369-385 (1981).
17. R. Skalak, A. Tozeren, R. P. Zarda, and S. Chien, Strain energy function of red blood cell membranes, *Biophys. J*. **13**, 245-264 (1973).
18. Y. R. Kim and L. Ornstein, Isovolumetric sphering of erythrocytes for more accurate and precise cell volume measurement by flow cytometry, *Cytometry* **3**, 419-427 (1983).
19. N. Mohandas, Y. R. Kim, D. H. Tycko, J. Orlik, J. Wyatt, and W. Groner, Accurate and independent measurement of volume and hemoglobin concentration of individual red cells by laser light scattering, *Blood* **68**, 506-513 (1986).
20. V. P. Maltsev and K. A. Semyanov, Characterization of bioparticles from light scattering (Vista Science Press, Netherlands, 2004).
21. B. H. Davis, Diagnostic utility of red cell flow cytometric analysis, *Clin. Lab Med.* **21**, 829-840 (2001).
22. L. K. Jennings, L. K. Brown, and M. E. Dockter, Quantitation of protein 3 content of circulating erythrocytes at the single-cell level, *Blood* **65**, 1256-1262 (1985).

23. S. J. Nance, Flow cytometry related to red cells, *Transfus. Sci.* **16**, 343-352 (1995).
24. N. J. Nusbaum, Red cell age by flow cytometry, *Med. Hypotheses* **48**, 469-472 (1997).
25. V. P. Maltsev, Scanning flow cytometry for individual particle analysis, *Rev. Sci. Instruments* **71**, 243-255 (2000).
26. M. I. Tiirikainen, Evaluation of red blood cell lysing solutions for the detection of intracellular antigens by flow cytometry [see comments], *Cytometry* **20**, 341-348 (1995).
27. V. L. Lew and R. M. Bookchin, Volume, pH, and ion-content regulation in human red cells: analysis of transient behavior with an integrated model, *J. Membr. Biol.* **92**, 57-74 (1986).
28. M. D. Sass, Effect of ammonium chloride on osmotic behavior of red cells in nonelectrolytes, *Am. J. Physiol* **236**, C238-C243 (1979).
29. R. J. Labotka, W. Galanter, and V. M. Misiewicz, Erythrocyte bisulfite transport, *Biochim. Biophys. Acta* **981**, 358-362 (1989).
30. K. A. Semyanov K. A. and P. A. Tarasov, Measurement of mammalian erythrocyte indices from light scattering with scanning flow cytometer, in *Diagnostic Optical Spectroscopy in Biomedicine* II. Edited by Wagnieres, Georges A. Proceedings of the SPIE, **5141,** 106-113 (2003).
31. K. A. Semyanov, P. A. Tarasov, A. E. Zharinov, A. V. Chernyshev, A. G. Hoekstra, and V. P. Maltsev, Single-particle sizing from light scattering by spectral decomposition, *Appl. Opt.* **43**, 5110-5115 (2004).
32. P. A. Tarasov, Study of characteristic parameters of population of human erythrocytes using dynamic flow cytometry, [in Russian], PhD thesis, Krasnoyarsk, 2005.
33. M. I. Mishchenko, L. D. Travis, and D. W. Mackowski, T-matrix computations of light scattering by nonspherical particles: A review, *J. Quant. Spectrosc. Radiat. Transf.* **55**, 535-575 (1996).
34. http://www.giss.nasa.gov/~crmim/